Real examples of surface reconstructions determined by direct methods

2002 J. Phys.: Condens. Matter 14 4075

(http://iopscience.iop.org/0953-8984/14/16/302)

INSTITUTE OF PHYSICS PUBLISHING JOURNAL OF PHYSICS: CONDENSED MATTER

J. Phys.: Condens. Matter **14** (2002) 4075–4086 PII: S0953-8984(02)29377-7

Real examples of surface reconstructions determined by direct methods

X Torrelles[1,9], J Rius[1], A Hirnet[2], W Moritz[2], M Pedio[3], R Felici[4], P Rudolf[5], M Capozi[6], F Boscherini[7], S Heun[3], B H Mueller[3] and S Ferrer[8]

[1] Institut de Ciència de Materials de Barcelona (CSIC), 08193 Bellaterra, Barcelona, Spain
[2] Institut für Kristallographie und Angewandte Mineralogie, Universität München, Theresienstr. 41, D-80333 München, Germany
[3] Laboratorio TASC-INFM, Area Science Park, SS 14, Km 163.5, 34012 Trieste, Italy
[4] INFM, Op. Group in Grenoble, c/o ESRF, 6 rue Jules Horowitz, Bp 220, F-38043, Grenoble Cedex, France
[5] LISE Facultes Universitaires Notre-Dame de la Paix, Namur, Belgium
[6] ISM-CNR, Area della Ricerca Tor Vergata, V Fosso del Cavaliere 100, 00100 Roma, Italy
[7] INFM, Dipartimento di Fisica, University of Bologna, viale C Berti Pichat 6/2, 40127 Bologna, Italy
[8] ESRF, 6 rue Jules Horowitz, Bp 220, F-38043, Grenoble Cedex, France

E-mail: xavier@icmab.es

Received 2 October 2001, in final form 27 November 2001
Published 11 April 2002
Online at stacks.iop.org/JPhysCM/14/4075

Abstract

In this work the modulus sum function is briefly introduced and its applicability to the automated interpretation of projections of reconstructed surfaces shown. The selected real examples have been arranged according to the interpretation complexity of the respective two-dimensional Patterson maps and correspond to the most common types of surface reconstructions represented by: (i) a shift of the surface atoms from their ideal positions. This type of reconstruction is often found on (001) semiconductor surfaces and its most characteristic structural feature is the pairing of neighbouring surface atoms forming dimers, e.g., the $In_{0.04}Ga_{0.96}As(001)$-$p(4 \times 2)$ reconstructed surface. (ii) Different atom types occupying the surface sites. This type of reconstruction can be induced by both the adsorption of deposited atoms onto the surface, e.g. Sb/Ge(113)-$c(2 \times 2)$, or a new structural arrangement of the substrate caused by the adsorption of external molecules onto the surface, e.g. C_{60}/Au(110)-$p(6 \times 5)$ reconstructed surface.

(Some figures in this article are in colour only in the electronic version)

[9] Author to whom any correspondence should be addressed.

1. Introduction

As is well known, the intensity in a surface diffraction experiment is distributed forming a periodic arrangement of so-called *diffraction rods*, the continuity of which in the direction normal to the surface reflects the lack of periodicity in this direction. When the surface relaxes, the diffracted intensities always have contributions from the bulk crystal and from the outer atoms, giving rise to a particular sort of rods called crystal truncation rods (CTRs). In contrast, when the surface reconstructs the associated symmetry reduction produces an additional set of rods called fractional-order rods (FORs) that just possess contributions of those atoms which take part in the reconstruction i.e. they contain no bulk information.

Traditionally, the first step in the structure solution of reconstructed surfaces has been the calculation of the projected difference Patterson function $[\delta P(u, v)]$. In the computation of this function only the intensities of the in-plane reflections are used, i.e. those points of the FORs with almost negligible perpendicular momentum transfer components. For simple reconstructions, interpretation of the $\delta P(u, v)$-function directly from the interatomic vectors found in the Patterson map provides projected models of the reconstruction that can be expanded along the surface normal to adjust the total three-dimensional measured data set. However, the difficulty for the direct interpretation of the partial Patterson maps increases as the number of atoms involved in the reconstruction becomes larger, so that, frequently, the interpretation is more like a trial-and-error comparison between diffracted intensities and intensities calculated from multiple models. In such complicated cases, powerful procedures for the automated $\delta P(u, v)$-function unravelling are required. Nowadays, two principal strategies exist to extract from the measured intensities the phase information lost during the diffraction experiment. One strategy takes advantage of the known bulk contribution to the CTRs to derive the unknown surface contributions (amplitudes and phases for the CTRs and only phases for the FORs). The second strategy is closer to conventional direct methods. Here, the phase information of the surface structure is derived from the measured intensities of the FORs, exclusively, so that the CTRs are only used to place the surface structure with respect to the bulk. The direct methods modulus sum function (MSF), the application of which to real examples is shown in this work, follows this second strategy. Up to now, all applications of the MSF have been with in-plane intensity data. The principal reason for this has been the difficulty to measure full data sets owing to the limited measuring time available when using synchrotron radiation sources. In the following sections, a short description of the MSF will be given and its application to three real examples of increasing difficulty will be analysed.

2. The direct methods MSF

The finality of the application of the MSF is the determination of the phases of the in-plane reflections. It is assumed that the set of refined phase values which maximizes MSF is correct. A Fourier summation including only these type of reflections will produce a two-dimensional partial electron density map consisting of positive and negative peaks. This partial electron density distribution is called difference function (δ) and is defined as $\delta(x, y) = \rho_R(x, y) - \langle \rho_R(x, y) \rangle$. $\rho_R(x, y)$ is the projected electron density distribution of the reconstructed surface, while $\langle \rho_R(x, y) \rangle$ is obtained after averaging the electron density ρ_R of the reconstruction over all the (1×1) subcells. Knowledge of δ allows, in most cases, the fast identification of the basic features of the surface structure. In addition to the availability of the in-plane structure factor moduli, one basic requirement for the success of the MSF is that δ fulfils the peakness condition. As recently shown [1], then, and only then, maximization of MSF which is defined by

$$\mathrm{MSF}(\Phi) = \Sigma_{\boldsymbol{H}}[|E(\boldsymbol{H})| - \langle|E|\rangle] \cdot |E(\boldsymbol{H}, \Phi)| = \mathrm{Max!}. \tag{1}$$

is essentially equivalent to minimization of the residual

$$R(\Phi) = \Sigma_{\boldsymbol{H}}[|E(\boldsymbol{H})| - |E(\boldsymbol{H}, \Phi)|]^2 = \mathrm{Min!} \tag{2}$$

between the observed and calculated $|E|$ magnitudes. The symbol Φ denotes the collectivity of refined phases φ of the strongest in-plane reflections $\boldsymbol{h}$. In (1) and (2), the summation extends over all measured in-plane reflections $\boldsymbol{H}$. In addition, to eliminate the 'form factor' and 'thermal vibration' fall-off, the structure factors $F(\boldsymbol{H})$ have been replaced in (1) and (2) by the normalized ones $E(\boldsymbol{H})$.

The critical point for the practical application of (2) is how to express $E(\boldsymbol{H})$ as a function of Φ. When, for example, the MSF is applied to single-crystal data, this is achieved via Sayre's equation which assumes that the electron density distribution ρ is similar to ρ^2 (and so their respective Fourier coefficients). Owing to the existence of positive and negative peaks in δ, δ and δ^2 are no longer alike, and consequently, the resemblance between δ and δ^3 is used instead. As shown in [2], this forces the introduction of an additional summation in Sayre's equation, so that $|E(\boldsymbol{H}, \Phi)|$ is given by

$$|E(\boldsymbol{H}, \Phi)| \propto \Sigma_{h'}\Sigma_{h''}|E(\boldsymbol{h}')||E(\boldsymbol{h}'')||E(\boldsymbol{H} - \boldsymbol{h}' - \boldsymbol{h}'')| \times \cos[\phi(-\boldsymbol{H}) + \varphi(\boldsymbol{h}') + \varphi(\boldsymbol{h}'') + \varphi(\boldsymbol{H} - \boldsymbol{h}' - \boldsymbol{h}'')] \tag{3}$$

where φ and ϕ denote the phases of the structure factors of δ and δ^3. Notice that the atomicity constraint is introduced by making in (3) ϕ equal to φ for the strongest in-plane reflections. Equation (3) can be computed easily for projections but becomes lengthy for three-dimensional data.

3. Application of the MSF

In this work, the MSF has been applied to several in-plane data sets to determine the projected structure of three surface reconstructions:

(1) The pairing of neighbouring surface atoms forming dimers on (001) semiconductor reconstructed surfaces: $In_{0.04}Ga_{0.96}As(001)-p(4 \times 2)$.
(2) The atomic arrangement of adsorbed atoms onto a substrate: Sb/Ge(113)-$c(2 \times 2)$.
(3) A new structural arrangement of the substrate surface induced by adsorbed molecules: C_{60}/Au(110)-$p(6 \times 5)$.

Each example contains a brief description of the preparation conditions and of the data acquisition procedure using grazing incidence surface x-ray diffraction (GIXD) techniques, followed by a comparison between the traditional solution methods, based on the interpretation of the projected $\delta P(u, v)$-function, and MSF methods applied both to the in-plane data. The examples are ordered according to the difficulties for interpreting their respective two-dimensional Patterson maps.

3.1. $In_{0.04}Ga_{0.96}As(001)$-$p(4 \times 2)$

3.1.1. Experimental. The samples were obtained by solid source molecular-beam epitaxy [3,4]. GaAs buffer layers 500 nm thick were initially grown at 600 °C on semi-insulating GaAs(001) wafers. $In_{0.04}Ga_{0.96}As$ epilayers 2 μm thick and forming a (2×4) surface reconstruction were subsequently grown at 500 °C with a III/V beam pressure ratio of approximately 1:40 [5]. For the transport, the samples were capped and cleaned by annealing up at 450 °C; during decapping the symmetry of the surface reconstruction evolved from

(2×4) to (4×2), at which point annealing was stopped. The $In_{0.04}Ga_{0.96}As$ diffraction experiment was carried out at the surface diffraction beamline ID3 of ESRF [6] at an energy of 16.0 keV.

The real-space basis is described by the lattice vectors $\boldsymbol{a}_1$ and $\boldsymbol{a}_2$ along $[1, -1, 0]$ and $[1, 1, 0]$, respectively, and with $\boldsymbol{a}_3$ taken perpendicular to the surface. Their magnitudes are $a_1 = a_2 = a$ (4.011 Å) and $a_3 = a_o$ (bulk constant) = 5.672 Å. The symmetry of the diffraction pattern is mm. Inspection of diffraction data along $\boldsymbol{a}_1^*$ showed well defined peaks at positions that were multiples of $1/4$. However, along $\boldsymbol{a}_2^*$, the half-order peaks were too diffuse to be measured, thus indicating the presence of a strong disorder in this direction [7]. Hence, the measured in-plane superstructure intensity data only contain reflections of type ($H = m/4$, $K = n$) with m and n being integers, which can correspond either to a superstructure $p(4 \times 2)$ averaged in $\boldsymbol{a}_2$ (hereafter denoted by $p(4 \times 1)$), or to a superstructure $c(8 \times 2)$ averaged along $\boldsymbol{a}_1$ and $\boldsymbol{a}_2$ to give the same $p(4 \times 1)$ cell [8]. The total number of measured in-plane fractional order reflections is 151, which reduce to 35 non-equivalent reflections with resolution less than 1 Å.

3.1.2. Discussion. The difference Patterson map computed with the in-plane superstructure reflections assuming *pmm* symmetry is given in figure 1(a). As mentioned earlier, the presence of elongated and poorly defined peaks along $\boldsymbol{a}_2^*$, makes the direct interpretation of the Patterson map difficult. One possibility is comparison with the known Patterson maps from related systems [8, 9]. From this comparison the peaks due to the As dimers can be clearly identified. However, the rest of the peaks are not satisfactorily explained by any of these models, as for example the strong peak located at (0.425, 0) or the peaks located along $a_2 = 1/2$ which are weaker than the expected ones derived from the previous models [8, 9]. To interpret these additional peaks, that is for solving the projected superstructure, the δ-MSF was applied. figure 1(b) shows the δ Fourier map of the superstructure projection (averaged along $\boldsymbol{a}_2$) computed with the best set of refined phases. From its inspection, it follows that:

(a) the topmost layer is formed by As dimers (A in figure 2) [8].

(b) The Ga dimers are normal to the As dimers (B in figure 2). The two physically reasonable ways of placing the Ga dimers in the superstructure are (i) for $p(4 \times 2)$: with glide plane along $\boldsymbol{a}_2$ relating the two Ga dimers in a zigzag manner, as depicted in figure 2 (the existence of this plane requires the absence of half-order reflections along $\boldsymbol{a}_2^*$ with H being equal to 0); and (ii) for $c(8 \times 2)$: with a mirror plane relating the two neighbour Ga dimers, as proposed in [8] on the basis of scanning tunnelling microscopy images (not represented in figure 2).

(c) The δ-peak at $(1/2, 1/2)$, which corresponds to the (0.425, 0) peak in the Patterson map (figure 1(a)), is most probably due to an In enrichment at this site. The refinement of the site occupancy indicates a 30–50% In enrichment.

This interpretation was confirmed by refining the model not only with the in-plane data but also with the experimental (1, 0), (0, 1) and (1, 1) CTRs (155 additional observations) [10]. The number of refined variables was kept to a minimum (one scale factor, seven (x, y) parameters, nine (z) parameters and eight anisotropic thermal vibration coefficients). Figure 3 shows the results of the fit. Recently, Erkoç and Kötken [11] have investigated systematically the energetics of As terminated GaAs(001) surfaces confirming that the co-existence of As and Ga dimers at different atomic levels are energetically very probable.

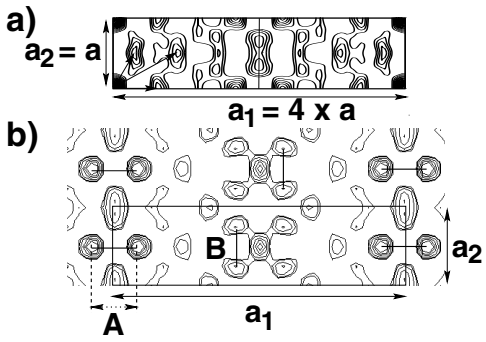

Figure 1. (a) Two-dimensional experimental Patterson function calculated with the measured intensities of the $In_{0.04}Ga_{0.96}As$ (001) in-plane superstructure reflections. (b) Difference map obtained from the phase refinement with the 'direct methods' difference sum function. Lines A and B indicate the As ad Ga dimers, respectively. Due to the half population of the Ga dimers, their peak strength is lower than for the As dimers.

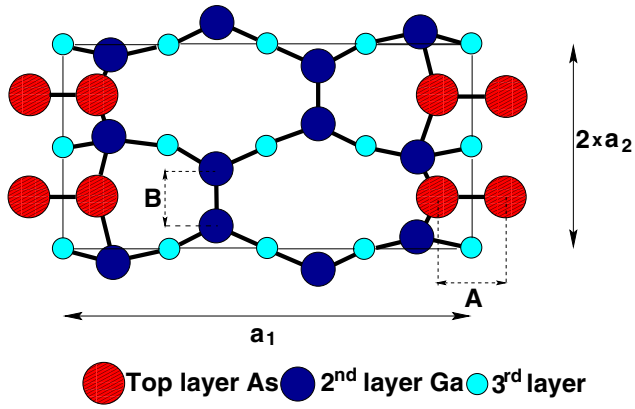

Figure 2. Projected 'ball and stick' model of the $p(4 \times 2)$ unit cell derived from the δ map in figure 1(b), assuming glide mirror along a_2 relating the Ga dimers ($p2mg$ symmetry).

3.2. Sb/Ge(113)-c(2×2)

3.2.1. Experimental. The bulk-terminated Ge(113) surface consists of a bilayer containing two different kinds of atoms and three dangling bonds per primitive (1×1) unit cell, one (111)-like atom with one dangling bond, and one (100)-like atom with two dangling bonds. The unreconstructed surface provides threefold coordinated adsorption sites that are well suited for the adsorption of group III or V metals.

The Ge(113) surface was cleaned in ultra-high vacuum (UHV) by Ar^+ ion bombardment at 900 K and subsequent annealing to 1050 K, followed by slow cooling to room temperature. After this treatment, the clean Ge(113) exhibits a surface reconstruction with sharp and strong (3×1) reflections and weak and diffuse (3×2) reflections. The Sb/Ge(113) was obtained after depositing 0.75 ML of Sb at 770–820 K followed by annealing at 1120 K. (1×2) spots as well as additional $c(2 \times 2)$ spots were detected by low-energy electron diffraction (LEED) [12]. The $c(2 \times 2)$ reflections were too weak to be measured by x-ray diffraction in reasonable timescales.

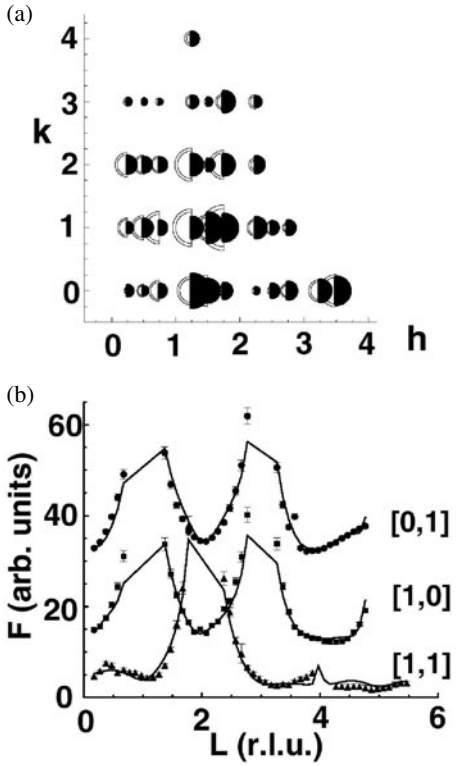

Figure 3. Observed (outer empty semicircles) and calculated (filled semicircles) structure factors of the in-plane superstructure reflections of $In_{0.04}Ga_{0.96}As$ (001)-$p(4 \times 1)$. The error bars of the data are proportional to the area between outer and inner radii (a). Observed and calculated CTRs (b). The structural refinement of the model shown in figure 2 includes four surface atomic levels.

Data collection of Sb/Ge(113)-$c(2 \times 2)$ was performed on a home-made UHV diffractometer [13] at the Wiggler beamline W1 at Hasylab using an energy of 10.3 keV.

The experimentally observed (1×2) unit cell of the Ge(113) surface was described in a centred orthogonal system by lattice vectors $\boldsymbol{a}_1$ and $\boldsymbol{a}_2$ parallel to $[1, -1, 0]$ and $[3, 3, -2]$, respectively, and with $\boldsymbol{a}_3$ perpendicular to the surface along $[1, 1, 3]$. Their magnitudes are $a_1 = a_o/\sqrt{2}$, $a_2 = 13.2683$ Å and $a_3 = \sqrt{11}a_o$ (a_o = bulk lattice constant: 5.658 Å).

The total number of non-equivalent measured fractional order in-plane reflections from the (1×2) superstructure is 59, figure 4 [12].

3.2.2. Discussion. The analysis of the in-plane dataset corresponding to the (1×2) unit cell was initially performed by direct interpretation of its computed two-dimensional Patterson map. The difference Patterson map corresponding to the (1×2) unit cell calculated from the in-plane data is shown in the figure 5(a). The difficulty of interpretation lead to several wrong models. For this reason the corresponding difference map was calculated with direct methods, figure 5(c). This map contains the average structural information of the $c(2 \times 2)$ superstructure projected into a (1×2) unit cell. The stronger peaks in the δ-map correspond to adsorbed Sb atoms and to topmost Ge atoms directly bonded to them showing maximum displacements from their 'ideal' bulk positions. From this interpretation a projected model containing three adsorbed Sb atoms can be easily obtained, figure 5(b). The Ad1,2 and Ad3 Sb atoms are threefold coordinated while the Int atoms are interstitial Sb dimers.

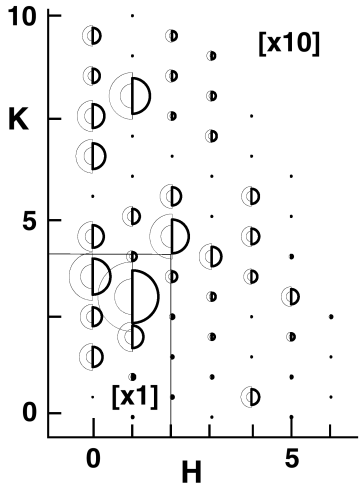

Figure 4. In-plane structure factors amplitudes corresponding to the Sb/Ge(113)-(1 × 2) surface reconstruction. The measured values and their associated uncertainties are proportional to the radii of the two empty semicircles. The right empty semicircles are proportional to the calculated values using the model shown in figure 5(b). Note that two different scales are used in the figure.

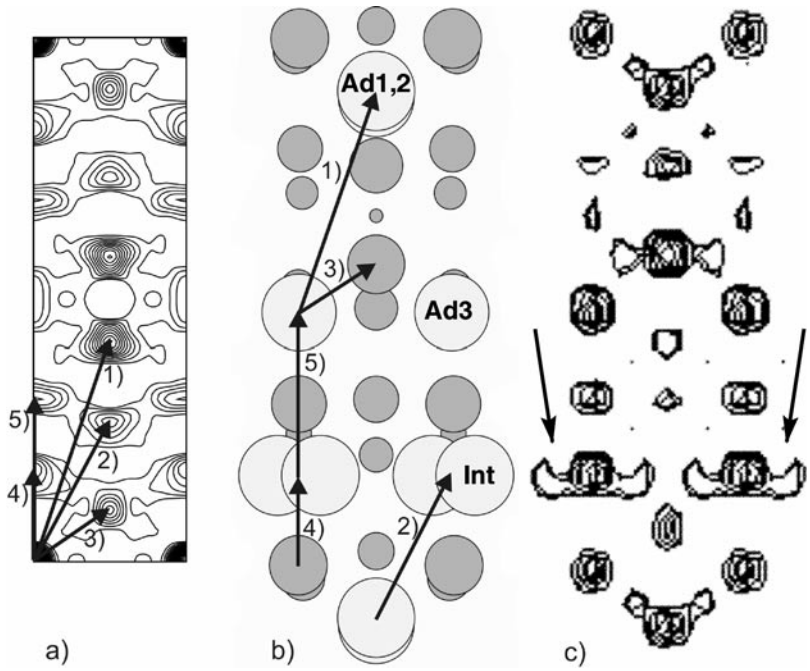

Figure 5. (a) Two-dimensional Patterson map obtained from the in-plane data of the $p(1 \times 2)$ Sb/Ge(113) superstructure. (c) Contour difference map obtained from in-plane data. (b) Top view projection of the model obtained after interpretation of the δ-map.

The best agreement between calculated and experimental data is obtained for a $c(2 \times 2)$ model proposed by Dabrowski *et al* [14] on the Sb/Si(113) system which is equivalent to that obtained from direct methods, figure 5(c). The average position of the $c(2 \times 2)$ Sb dimers in

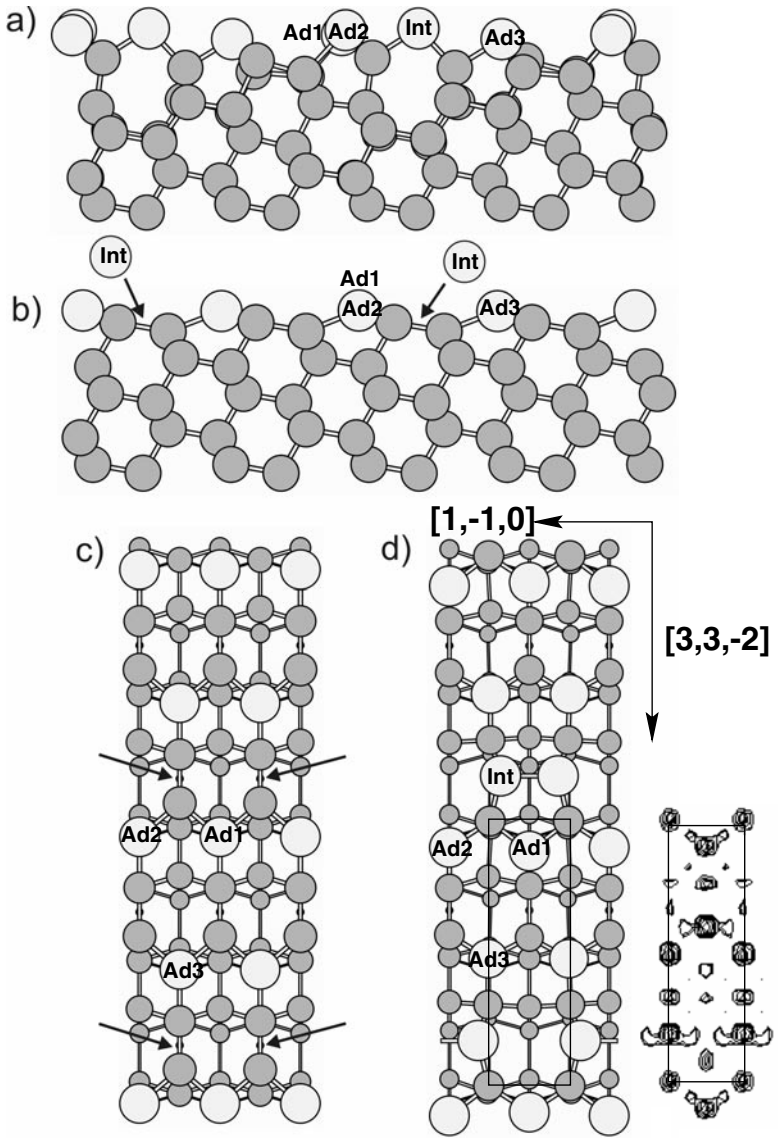

Figure 6. The $c(1 \times 1)$ structure is formed after depositing 0.5 ML of Sb onto a Ge(113) surface (b) and (c). The adsorption of Sb atoms on threefold coordinated places induces stress on the first surface layer. The surface stress is reduced by a breaking of the Ge–Ge bond (arrows) and inserting an additional Sb interstitial atom there. The $c(2 \times 2)$ structure is obtained after depositing 0.75 ML of Sb (a) and (d). This model was refined after expanding to a $c(2 \times 2)$ surface cell the model shown in figure 5(b) and refining it using the full data set measured. The (1×2) unit cell has been outlined on the $c(2 \times 2)$ structure to better distinguish the similarities between the true structure and the difference map.

the smaller (1×2) unit cell causes the peak splitting (indicated with arrows) in the difference map. The refined structure using the full dataset (100 additional out-of-plane reflections) is showed in figure 6.

As can be seen from this figure, the structural differences between the $c(2 \times 2)$ and the (1×2) reconstructions are very small and are practically due to the two Sb dimers in the

$c(2 \times 2)$ unit cell. Figures 6(b) and (c) show a lateral and top projections, respectively, of the $c(1 \times 1)$ surface reconstruction due to Sb adatoms on the Ge(113) surface after depositing 0.5 ML of Sb. In this structure, the Sb atoms are located in threefold coordinated sites, which induce strong tensions in the first surface layer. The Sb–Ge and Ge–Ge bonds reveal a strong expansion of 12% along [3, 3, −2] [15]. The adsorption of 0.25 ML of Sb (Int) suppresses these tensions since these new Sb atoms occupy interstitial sites, thus breaking the high stressed Ge–Ge bonds. These two adjacent Sb atoms form a Sb dimer. Figures 6(a) and (d) show lateral and top views, respectively, of the $c(2 \times 2)$ superstructure (obtained after depositing 0.75 ML of Sb). The diffuse streaks in the LEED pattern can be easily explained by the ordering of the interstitial dimers. The dimer rows along [1, −1, 0] are internally well ordered, while different dimer rows are only weak correlated. The weak interaction is caused by their long distance (6.63 Å) along [3, 3, −2].

3.3. C_{60}/Au(110)-$p(6 \times 5)$

3.3.1. Experimental. The clean Au(110) surface is very anisotropic since it exhibits a (1×2) missing row reconstruction [16] where one of every two closest-packed atomic rows along [1, −1, 0] is missing. The structure of C_{60} monolayers is usually hexagonal or quasihexagonal resulting in compressed or enlarged C_{60}–C_{60} spacings compared to the C_{60} solid in order to achieve commensurate structures [17–19]. Moreover, C_{60} is also capable of inducing strong structural modifications in a metal substrate as recently demonstrated by scanning tunnelling microscopy (STM) on C_{60}/Ni(110) [20] which reveals that different adsorbate phases are formed within a general roughening and restructuring of the interface resulting in the formation of (100) microfacets.

In the thermodynamically stable adsorption of C_{60} on Au(110), the part of the Au surface covered with an hexagonal close-packed corrugated monolayer of C_{60} shows a (6×5) reconstruction while those areas of the substrate not covered by the adsorbate exhibit a (1×5) missing row reconstruction as previously determined by STM [21]. The fact that the corrugation of the C_{60} monolayers is comparable to the difference in heights of the (1×2) and (1×3) missing row structures, which constitute the basis for the (1×5) reconstruction, leads the authors to conclude that the (1×5) Au reconstruction extends below the C_{60} layer.

The C_{60}/Au(110)-$p(6 \times 5)$ diffraction experiment was carried out at the surface diffraction beamline ID3 (ESRF) [6] using an energy of 13.4 keV. The Au(110) crystal was mounted in a UHV diffraction chamber (10^{-10} mbar range) where the Au(1×2) reconstructed surface was prepared. C_{60} was sublimated from a Ta-crucible kept at 750 K and its coverage was determined by Auger spectroscopy [22–24]. After adsorption at room temperature of two layers of C_{60} onto the Au substrate, the sample was annealed to 600 K until a well (6×5) structure was observable.

The real-space basis of the Au(110) surface is described by the lattice vectors $\boldsymbol{a}_1$ and $\boldsymbol{a}_2$ which are parallel to [1, −1, 0] and [0, 0, 1], respectively, and with $\boldsymbol{a}_3$ perpendicular to the surface along [1, 1, 0]. Their magnitudes are $a_1 = a_3 = a_o/\sqrt{2}$, $a_2 = a_o$ (a_o = bulk lattice constant). The total number of measured in-plane reflections of the (6×5) reconstruction is 300, which reduce to 130 independent reflections according to *mm* symmetry, figure 7 (empty semicircles). Reflections of type $(H, 0)$ with $H = (2n + 1)/6$ and n = integer are systematically absent which indicates the presence of a glide line along $\boldsymbol{a}_1$, thus suggesting *pmg* as the most probable plane group for the reconstruction.

Analysis of the intensity statistics indicates that the reflections of type (1×5) are 35% stronger than the rest thus also suggesting the existence of (1×5) regions. Consequently, they were excluded from the calculations.

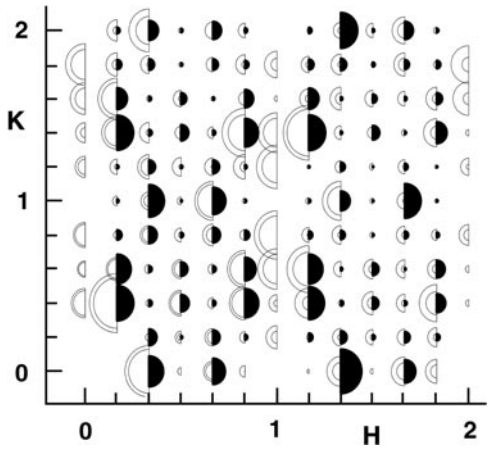

Figure 7. In-plane structure factors amplitudes corresponding to the C_{60}/Au(110)-$p(6\times5)$ surface reconstruction. The measured values and their associated uncertainties are proportional to the radii of the two empty semicircles. The filled semicircles are proportional to the calculated values using the model shown in figure 9(b). This model was not used to calculate the values of the integer H-reflections because these data were not used in the computation of the 'direct methods' difference sum function.

3.3.2. Discussion. The available model proposed by the STM analysis [21] (figure 9(a)) was refined using *pmg* symmetry and with 28 positional parameters. The refinement resulted in unrealistic in-plane Au displacements with a poor agreement between the calculated and experimental data.

Standard procedures routinely employed in surface crystallography such as direct interpretation of the experimental projected difference Patterson map (figure 8(a)), proved to be useless due to the complexity involved. This is becoming a common problem when solving complex reconstructed surfaces of adsorbate–substrate systems. For this reason it was decided to derive the phases of the largest structure factors with the δ-MSF [2]. The projected δ-map for the best solution (assuming *p1g* symmetry) is given in figure 8(b).

Comparison of figures 8(a) and (b) clearly illustrates the difficulty to interpret the Patterson map. Inspection of the stronger peaks in the δ-map indicates the presence of a mirror line normal to $\boldsymbol{a}_1$ leading us to conclude that the true in-plane symmetry is most probably *pmg*. The simplest model that explains the most intense δ peaks, located along rings with a diameter of about 9.6 Å and marked as dashed lines in figure 8(b), is represented in figure 9(b). This model implies the fullerene-induced reconstruction is accompanied by a very important mass redistribution within the unit cell since all compact atomic rows along the $\boldsymbol{a}_1$ direction in the second layer have missing atoms. The Au atomic positions of the $p(6\times5)$ model proposed in figure 9 are in bulk crystal lattice positions. This model was refined using the 108 in-plane reflections to a reduced $\chi^2 = 3.5$ (eight structural fit parameters, one scale factor and one global temperature factor for the topmost atoms). The maximum rms deviation of the fitted coordinates from the ideal values is 0.2 Å. In spite of the limited number of refined variables, the agreement is rather remarkable as it can be seen from figure 7 where the filled semicircles are proportional to the structure factor amplitudes calculated with the proposed model. The calculation ignored the fullerenes since their scattering factor is very weak compared to that of the Au atoms [25], especially at moderate and high resolutions.

The proposed structure [26] implies corrugation of the C_{60} overlayer in agreement with STM results and reveals that the C_{60} adsorption is accompanied by important displacements

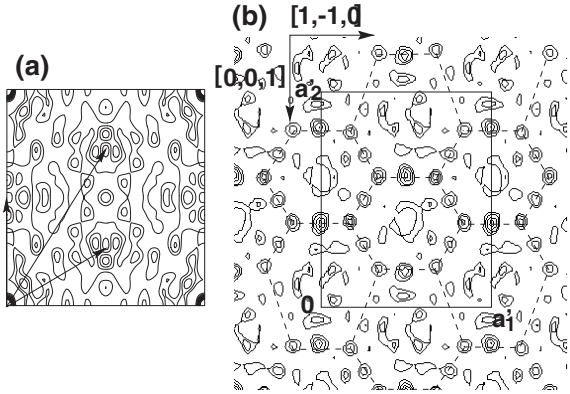

Figure 8. (a) Two-dimensional data Patterson map computed from the measured in-plane dataset. Arrows indicate the position of the fullerene molecules in the unit cell. (b) Contour difference map (positive regions) of C_{60}/Au(100)-$p(6\times5)$ obtained by applying the 'direct methods' difference sum function to the partial set of in-plane reflections given in figure 8 (see text for details). Dashed lines indicate the locations of the C_{60} molecules. The rectangle outlines the 6×5 unit cell (17.3×20.4 Å^2).

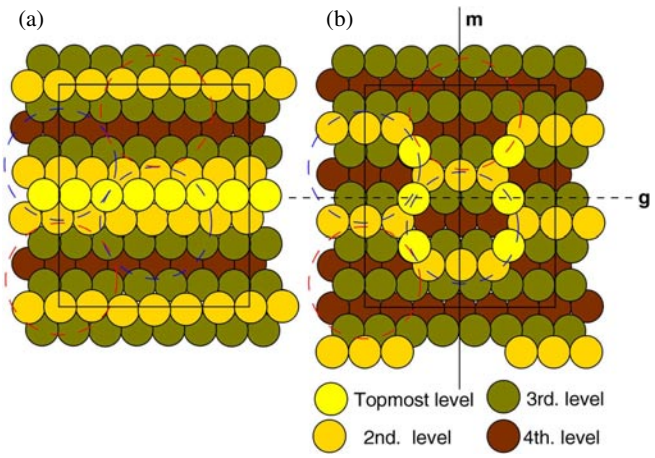

Figure 9. (a) Top-view projection of the C_{60}/Au(110)-$p(6\times5)$ surface reconstruction model obtained from STM measurements [21]. The relative heights of the Au atoms are indicated by different colours (darker shades represent deeper atoms). The fullerenes are indicated by the dashed circles. (b) Top-view projection of the C_{60}/Au(110)-$p(6\times5)$ surface reconstruction model obtained from the direct interpretation of the difference map, figure 8(b). Lines m and g indicate a mirror and a glide line, respectively.

of underlying Au atoms, leading to a calyx-shaped arrangement to accommodate better the fullerene molecules situated at (0, 0.6) and (1/2, 0.4) (blue dashed circles). The C_{60} molecules at (0, 0.1) and (1/2, 0.9) (red dashed circles) have more space and rest directly on the low-level Au atoms. Accordingly, the adsorbate overlayer is composed of zigzag and buckled rows since the fullerenes (0, 0.6) and (1/2, 0.4) are expected to be one atomic level higher than the (0, 0.1) and (1/2, 0.9) ones.

4. Conclusions

The δ-MSF has been successfully applied to the $In_{0.04}Ga_{0.96}As(001)$-$p(4 \times 2)$, Sb/Ge(113)-$c(2 \times 2)$ and C_{60}/Au(110)-$p(6 \times 5)$ reconstructed surfaces. The corresponding difference maps are easier to interpret than the respective Patterson maps which permits the finding of new models for adjusting the experimental data. The lower level of difficulty for a correct interpretation of the δ-maps, since their peaks can be directly assigned to atomic positions in the unit cell against interatomic vectors in the Patterson maps, permits the analysis of larger and difficult reconstructed surfaces. The sensitivity of these new methods to incomplete datasets, mainly to the systematic omission of reflections, provides average information of the structure that sometimes is insufficient for solving the structure, as it has been shown in the first example of this work.

Acknowledgment

XT and JR acknowledge the financial support of DGES (MEC), Project no PB98-0483.

References

[1] Rius J, Torrelles X, Miravitlles C, Amigó J M and Reventós N M 2002 *Acta Crystallogr.* A **58** 21
[2] Rius J, Miravitlles C and Allmann R 1996 *Acta Crystallogr.* A **52** 634
[3] Bonani A, Vanzetti L, Sorba L, Franciosi A, Lomascolo M, Prete P and Cingolani R 1995 *Appl. Phys. Lett.* **66** 1092
[4] Nicolani R *et al* 1994 *Phys. Rev. Lett.* **72** 294
[5] Paul S, Roy J B and Basu P K 1991 *J. Appl. Phys.* **69** 827
[6] Ferrer S and Comin F 1995 *Rev. Sci. Instrum.* **66** 1674
[7] Sauvage-Simkin M, Garreau Y, Pinchaux R, Veron M B, Landesman J P and Nagle J 1995 *Phys. Rev. Lett.* **75** 3485
[8] Skala L, Hubacek J S, Tucker J R, Lyding J W, Chou S T and Cheng K Y 1993 *Phys. Rev.* B **48** 9138
[9] Northrup J E and Froyen S 1994 *Phys. Rev.* B **50** 2015
[10] Torrelles X, Rius J, Boscherini F, Heun S, Mueller B H, Ferrer S, Álvarez J and Miravitlles C 1998 *Phys. Rev.* B **57** R4281
[11] Erkoç S and Kökten H 2000 *Int. J. Mod. Phys.* C **11** 1225
[12] Hirnet A 2000 *Dissertation* Institut für Kristallographie and Angewandte Mineralogie University of Munich, Germany
[13] Albrecht M, Antesberger H, Moritz W, Plöckl H, Sieber M and Wolf D 1999 *Rev. Sci. Instrum. V* **70** 3239
[14] Dabrowski J, Müssig H-J, Wolf G and Hinrich S 1998 *Surf. Sci.* **411** 54
[15] Hirnet A, Gierer M, Albrecht M, Schroeder K, Blügel S, Torrelles X and Moritz W, to be published
[16] Copel M and Gustafsson T 1986 *Phys. Rev. Lett.* **57** 723
[17] Rudolf P, Gensterblum G and Caudano R 1997 *J. Phys. (Paris), Collq.* **7** C6–136
[18] Rudolf P 1996 *Fullerenes and Fullerene Nanostructures* ed H Kuzmany, J Fink, M Mehring and S Roth (Singapore: World Scientific) p 263
[19] Maxwell A J, Brühwiler P A, Arvanitis D, Hasselström J, Johansson M K-J and Martensson N 1998 *Phys. Rev.* B **57** 7312
[20] Murray P W, Pedersen M O, Laegsgaard E, Stensgaard I and Besenbacher F 1997 *Phys. Rev.* B **55** 9360
[21] Gimzewski J K, Modesti S and Schlittler R R 1994 *Phys. Rev. Lett.* **72** 1036
[22] Maxwell A J, Brühwiler P A, Nilsson A, Martensson N and Rudolf P 1994 *Phys. Rev.* B **49** 10 717
[23] Modesti S, Cerasari S and Rudolf P 1993 *Phys. Rev. Lett.* **71** 2469
[24] Pedio M, Grilli M L, Ottaviani C, Capozi M, Quaresima C, Perfetti P, Thiry P A, Caudano R and Rudolf P 1995 *J. Electron. Spectrosc. Relat. Phenom.* **76** 405
[25] Torrelles X, Rius J, Pedio M, Felici R, Rudolf P, Alvarez J, Ferrer S and Miravitlles C 1999 *Phys. Status Solidi* b **215** 773
[26] Pedio M, Felici R, Torrelles X, Rudolf P, Capozi M, Rius J and Ferrer S 2000 *Phys. Rev. Lett.* **85** 1040